Journal Pre-proof

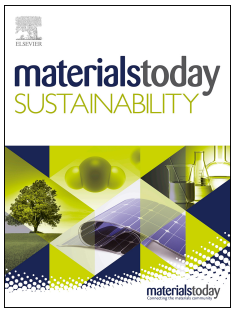

Multifunctional metal-free rechargeable polymer composite nanoparticles boosted by CO_2

Amparo Fernández-Benito, Giovanna Rodríguez, Daniel Arenas-Esteban, Martin Sjödin, Paula Navalpotro, Daniel Rodríguez-Caballero, David Ávila-Brande, Miguel Ángel López-Manchado, Javier Carretero-González

PII: S2589-2347(20)30017-8

DOI: https://doi.org/10.1016/j.mtsust.2020.100048

Reference: MTSUST 100048

To appear in: *Materials Today Sustainability*

Received Date: 19 March 2020

Revised Date: 28 May 2020

Accepted Date: 30 June 2020

Please cite this article as: A. Fernández-Benito, G. Rodríguez, D. Arenas-Esteban, M. Sjödin, P. Navalpotro, D. Rodríguez-Caballero, D. Ávila-Brande, M.Á. López-Manchado, J. Carretero-González, Multifunctional metal-free rechargeable polymer composite nanoparticles boosted by CO_2, *Materials Today Sustainability*, https://doi.org/10.1016/j.mtsust.2020.100048.

J.C.G. supervised the project and conceived the idea. A.F.B., G.R., and D.R.C. designed and performed the materials synthesis experiments and characterization with assistance from M.L.M. and J.C.G. A.F.B. and M.S. performed the electrochemical characterization experiments of the suspensions containing the hierarchically structured polymer composite and the solid-state polymer composite electrodes, respectively. D.A.E. and D.A.B. performed TEM studies. P.N. performed the analysis of the CV to estimate the reversible charge storage capacity. A.F.B. and J.C.G. wrote the manuscript with input from all co-authors.

Multifunctional metal-free rechargeable polymer composite nanoparticles boosted by CO_2

Amparo Fernández-Benito,[a] Giovanna Rodríguez,[a] Daniel Arenas-Esteban,[b] Martin Sjödin,[c] Paula Navalpotro,[a] Daniel Rodríguez-Caballero,[a] David Ávila-Brande,[b] Miguel Ángel López-Manchado[a] and Javier Carretero-González[a,*]

[a] Institute of Polymer Science and Technology (ICTP-CSIC), Madrid, Spain
[b] Department of Inorganic Chemistry, Faculty of Chemistry, Universidad Complutense de Madrid, Madrid, Spain
[c] Department of Engineering Sciences, Uppsala University, Uppsala, Sweden

Abstract

Herein, we present a multigram scale-up route for the preparation of novel polymer composite nanoparticles as potential multifunctional rechargeable material for future, sustainable batteries. The nanoparticles (20 nm) comprise three innocuous yet functional interpenetrated macromolecular networks: polypyrrole, methylcellulose, and lignin. They are uniquely assembled in strands or chains (~200 nm) such as *necklace beads* and show long-time stability as water dispersion. We find that an aqueous suspension of this hierarchical nanomaterial show two sets of reversible redox peaks, separated by~600 mV, originating from the catechol moieties present in the lignin biopolymer. Remarkably, addition of carbon dioxide increased the capacity of one of the redox processes by 500 %. Importantly, the three redox stages occur in the presence of the same nanostructured polymer so being a potentially bifunctional material to be used in advanced electrochemical systems. The new properties are attributed to an intrinsic chemical and electronic coupling at the nanoscale among the different building blocks of the metal-free polymer composite and the structural rearrangement of the interpenetrated polymer network by the incorporation of CO_2. We have provided both a new electrochemically multifunctional hierarchically-structured material and a facile route that could lead to novel sustainable energy applications.

Keywords: multifunctional electrolyte, energy storage, CO_2 utilization, polymer nanomaterials, flow batteries.

INTRODUCTION

The increase of pollution levels in the atmosphere and their global impact on human health and on climate change are pushing rapid integration of energy from wind and sun into the electric grid as well as the electrification of the transport sector [1]. In addition, to reach a low-carbon and climate-resilient future, highly efficient, low-cost and large-scale methods to decrease the CO_2 concentration in urban and industrial areas are also needed [2]. Batteries have not yet achieved the degree of versatility and functionality to, simultaneously, store electricity and CO_2. In addition, the use of more sustainable energy storage materials to minimize the original carbon dioxide footprint of fabricating and recycling the battery is highly needed [3].

In search for superior battery performance, one of the strategies adopted by researchers has been the development of electroactive materials structured on the nanometer scale [4]. By diminishing particle sizes [5] or the layer thickness [6] to nanometer size, the solid state ion diffusion distances decrease while the surface area increases, thus enabling capacity values close to the theoretical ones even at high cycling rates. Nanostructured electrodes can also accommodate large strain without pulverization, providing mechanical flexibility and sustained electronic contact under stress [7].

However, the fabrication of nanostructured electrodes and electroactive nanoparticles normally involves complex synthetic routes with several reaction steps and often with the use of harmful chemicals. Moreover, these methods usually provide a very low amount of functional material making the overall process highly costly and difficult to up-scale. The electroactive nanoparticles are usually of low density resulting in challenges to pack them into highly compact electrodes and thus diminishing the possibility to enhance the volumetric energy density of the battery.

From a practical point of view, if the solid electrodes in a conventional secondary battery (Scheme 1A) were fractionated into a large amount of nanoparticles (Scheme 1B) and dispersed in a liquid solvent, an increase in both capacity and power capability of the battery might be expected. The main reason for this is the decreased restrictions due to the length scales for ion insertion, which are

reduced to short distances. The use of redox nanoparticles is becoming crucial in controlling the amount of charge stored by utilizing various charge storage mechanisms such as surface-based ion-adsorption, pseudocapacitance and diffusion-limited intercalation. Besides, a larger amount of energy than in conventional thin-film solid electrodes could be stored as mass transport can be achieved by forced convection. Moreover, if sufficiently dense the nanoparticles will ensure a high volumetric energy density too.

This description is closely related to what occurs in suspension electrode flow batteries [8]. The energy limitation of these systems is the dispersibility of the redox-active material in the liquid solvent. In most cases, researchers have implemented organic solvents [9] to maximize the concentration of the redox species and the voltage window; but the battery system would be expensive and unsafe if large volumes of flammable organic solvent are used. The utilization of organic solvents may also result in low ion mobility and poor rate capability [10]. Therefore, in order to achieve cost-efficient and safer electrochemical systems to store a large amount of energy from renewable sources, the use of water as the main solvent is desired. Recently, a flow battery based on a 1M aqueous dispersion of micro-sized redox-polymer-particulates have been developed showing excellent electrochemical properties with reversible, multi-electron redox processes, rapid electrochemical kinetics and ultra-stable, long-term cycling capability [11]. The application of electroactive polymer particulate slurries [11], solutions [12] or colloids electrolytes [13] also makes it possible to replace expensive ion-conducting membranes with much cheaper, commercial dialysis membranes operating through the size-exclusion mechanism (Scheme 1C). However, because a large number of redox-active materials are not soluble in water the dispersion and stabilization without using surfactants or emulsifiers will be challenging.

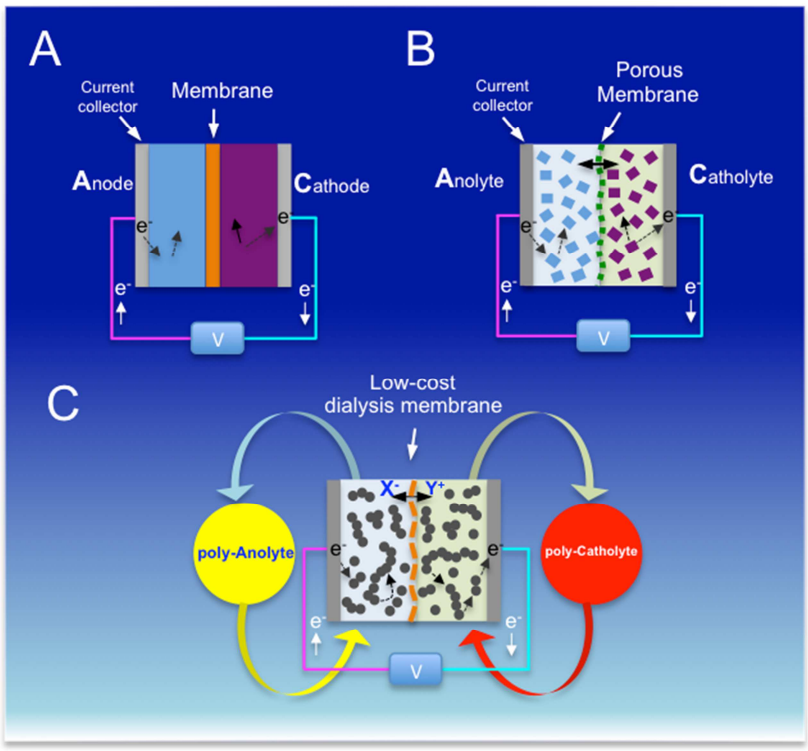

Scheme 1. Configurations of different electrochemical cells: conventional battery system with thick solid-state electrodes **A),** semi solid-like battery **B)** and a redox-active particulate electrolyte flow battery **C)**.

Herein, we have applied a sustainable route for the preparation of highly-water dispersible and electrochemically rechargeable polymer composite nanoparticles. This composite nanomaterial is composed of three different polymers and each polymer, in turn, is build-up solely of renewable, abundant and non-toxic building blocks. In this work, the selected methylcellulose has two functions: i) it assists the formation of nanoparticles during the colloidal polymerization; and ii) it brings about long-time stability of the suspensions in water. The other two functional components are lignin and polypyrrole. The former is the most abundant aromatic biopolymer on earth and can reversibly store charge through the reduction and oxidation of catechol moieties (Scheme 2) [14]. The latter is a low-cost biocompatible conjugated polymer that will enhance the charge transport properties in the composite nanomaterial. This new redox-active polymer composite is easy to prepare and its synthesis does not require additional metal or expensive components.

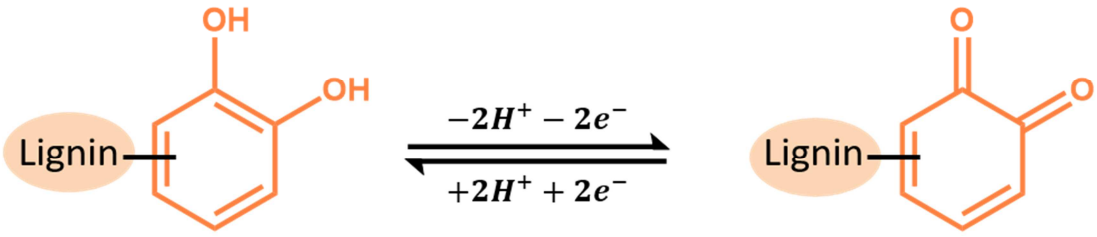

Scheme 2. Electrochemical oxidation and reduction of catechol moieties of lignin biopolymers in protic media.

Previous studies of polymer composites made from polypyrrole and cellulose derivatives [15] or redox- active lignin [6], have focused on their use as solid electrode materials. In this work, the redox chemistry of a stable suspension of interpenetrated lignin, cellulose and polypyrrole networks was exploited, making possible to trigger further functionality in these composites. In the presence of CO_2 two main processes, corresponding to the redox reactions of lignin occurring at different potentials were evidenced when electrochemically cycled in aqueous protic media. These two processes, observed in the cyclic voltammograms, are attributed to catechol moieties exhibiting different chemical substituents connected to the aromatic ring. In presence of CO_2, the electrochemical response of one of the processes is enhanced by up to 500 %. Thus, a novel highly-water dispersible metal-free polymer exhibiting three redox stages is presented. These results show the potential use of stable polymer composite suspensions as bifunctional single active material in flow systems operating under eco-friendly conditions.

EXPERIMENTAL SECTION

Preparation of the multifunctional polymer composites.

The preparation method for the multifunctional nanomaterials containing the three macromolecules was as follows: 0.16 g of methylcellulose (Sigma-Aldrich) was dissolved in deionized water (200 ml) at 60 °C during 60 minutes. After cooling down to room temperature, 1 g of lignin biopolymer (Sigma-Aldrich), with a variable content of sulphonic groups in its composition (see Table S1), 0.25 g of pyrrole monomer (Sigma-Aldrich) and 0.5 g of $FeCl_3$ (Sigma-Aldrich) as catalyst were added successively. Then, the mixture was stirred for 1 hour. The solution turned black immediately, signifying that the polymerization had

started and then after a few minutes a black solid precipitated to the bottom of the reaction flask. Subsequently, the solid was separated from the solution by centrifugation, washed with deionized water, and centrifuged again. This process was repeated up to three times. Next, the solid was freeze-dried overnight and stored at 2 °C until use. The terminology to designate the polymer composite samples was the following: *MPLX*, where *M*, *P*, and *L* mean methylcellulose, polypyrrole, and lignin, respectively, and *X* indicates the content of sulphonic groups in the lignin as estimated by the sulphur content derived from elemental analysis. So, *X* is designated as *L* when the amount of elemental sulfur in lignin is 1.6 wt. %, *M* means medium and corresponds to a content of 3.7 wt. % and *H* is used to denote the lignin with high sulfur content which is 4.9 wt. %. The composites containing either polypyrrole-lignin or a methylcellulose-polypyrrole couple are denoted *PLX* and *MP*, respectively.

Characterization of the polymer composites by electron microscopy.

The morphology and dimensions of the synthesized polymer composite materials were studied by using electron microscopy: scanning (SEM) and transmission (TEM). A high-resolution scanning electron microscopy (HRSEM) in a Hitachi S-8000 model with field emission filament and a voltage of 1.0 kV. For TEM studies, the polymer composite materials were ultrasonically dispersed in water. A few drops of the resulting suspension were deposited in a carbon-coated grid. TEM and high-angle annular dark-field imaging (HAADF) in Scanning Transmission Electron Microscopy (STEM) mode experiments were performed with a JEOL JEM 3000F microscope operating at 300 kV (double tilt (±20°) (point resolution 0.17 nm in TEM mode and 0.14 nm in STEM mode)), fitted with an X-ray energy dispersive spectroscopy (XEDS) microanalysis system (OXFORD INCA). The atomic ratio of the metals has been determined by XEDS. XEDS-mappings were recorded in ADF-STEM mode using the $K_{\alpha 1}$ lines of the elements with 256×256 pixel resolution accumulated over at least 1 hour to ensure good statistics.

Electrochemical characterization.

Preparation of polymer composite films for electrochemical analysis. 2.5 μL PLH or MPLH suspension was drop-casted onto freshly polished (0.3-micron alumina) gold-disc electrodes (Bio-Logic, A-002421 AUE Gold electrode (OD: 6 mm – ID: 3.0mm)) and the suspensions were allowed to dry over-night in ambient air. The PLH and MPLH layers were then characterized electrochemically in 1M $NaCl_{aq}$ electrolyte buffered with 10 mM Na_2HPO_4 and 10 mM H_3BO_3 to pH 4.3 and purged with N_2 for 20 min. The electrolyte was kept under a N_2 atmosphere throughout the measurement. A Pt wire (Bio-Logic, A-002234 Platinum counter electrode coiled, wire diameter 0.5 mm) immersed directly into the electrolyte solution was used as a counter electrode and an Ag/AgCl 3M NaCl (Bio-Logic, A-012167 RE-1B Reference Electrode) was used as the reference electrode. A CHI660 potentiostat was used for all measurements. All electrodes were characterized by cyclic voltammetry between -0.5 and 0.6 V at various scan rates. The quinone peak potentials were evaluated both for the oxidation (Ep_{Ox}) and the reduction (Ep_{Red}) peak by subtracting a linear base-line and fitting the peak to a Gaussian function. The average of the oxidation and reduction peak potential was taken as the quinone formal potential and the formal potential was evaluated at several scan rates together with the peak potentials. The formal potential (E'_o) for the different samples was derived by averaging the evaluated formal potentials at different scan rates. The dependence of the peak current with scan rate was investigated by determining the current at (Ep_{Ox}) and (Ep_{Red}), respectively.

Quinone and polypyrrole (PPy) content estimation in the thin film polymer composite electrodes. The total capacity was evaluated by integrating the anodic and cathodic sweeps at the lowest scan rate (0.01 V/s). Capacity originating from PPy was evaluated by subtracting the quinone capacity from the total capacity. Then, that value was multiplied by the weight percentage of PPy in the polymer composite estimated from the elemental analysis of nitrogen.

Electrochemical analysis of the polymer composite suspensions. Electrochemical studies of the polymer suspensions were performed by using a three-electrode configuration with porous graphite felt material as the working electrode, Ag/AgCl as a reference and platinum wire as a counter electrode. The graphite felt was thermally treated at 500 °C for 12 hours before use. The three-electrode

configuration cells were cycled in a VMP-300 multichannel potentiostat/galvanostat (Bio-Logic). The aqueous based-suspension was purged with N_2 gas for 20 minutes before measuring. The suspensions were titrated with dilute H_2SO_4 to the desired pH value at 25 °C. For the series of measurements performed with CO_2 gas, a flow of 80 ml/min (P_{CO2} = 1 atm and Tª = 25 ºC) was passed through a volume of 20 ml containing a suspension of nanoparticles dispersed in deionized water with a concentration of 1 gL^{-1} for 20 minutes. Then, the pH was adjusted following the same titration procedure as for the aqueous suspensions without CO_2.

Physical gas adsorption.

The textural properties of the polymer composites such as pore size, specific surface area, and pore volume were initially studied by N_2 gas adsorption at 77 K. This method is ideal for porous samples with a pore size in the range of 0.7-2 nm. However, we evidenced very low N_2 adsorption values, close to the instrumental detection limit, for all the polymer composite samples, most probably due to the presence of an average pore size smaller than 1 nm. CO_2 gas adsorption at 273 K was therefor used instead as CO_2 exhibits a smaller hydrodynamic radius and lower adsorption temperature than N_2 facilitating diffusion of gas molecules towards the surface. Both N_2 and CO_2 gas adsorption measurements were carried out by using Autosorb equipment (Quantachrome). The amount of sample used for each analysis was approximately 100 mg. The samples were degassed previously under vacuum for 12 hours before to start the gas adsorption isotherm. The measurements were performed at 273.15 K by applying a saturation pressure of CO_2 of 26142 torr. The relative pressures range for the adsorption was between 4.51 10^{-4} and 2.90 10^{-2} torr. The specific micropore surface area, average pore size, and micropore volume, were determined from the adsorption data using the Dubinin–Radushkevich and Stoeckli equations [16].

Ultraviolet-Visible (UV-Vis) spectroscopy.

Spectroscopic measurements were carried out in a quartz cuvette (optical path length of 10 mm) containing 0.1 g l^{-1} of the polymer composites, Lig-HS, and MP

in water solution. The electronic processes were monitored by using a Perkin Elmer model Lambda 35 spectrophotometer over the range 200-700 nm spectrum region.

Elemental analysis.

The content of C, H, S, and N in the polymer samples (5 mg) was determined by combustion in a LECO CHNS-932 thermal analyzer.

Dynamic Light Scattering (DLS) and zeta potential.

The average particle size and surface charge of the polymer composite materials were measured by DLS using a Malvern Nanosizer NanoZS Instrument equipped with a 4 mW He-Ne laser (λ = 633 nm) at a scattering angle of 173°. Different samples were measured in square polystyrene cuvettes (SARSTEDT) at 25 °C. The autocorrelation function was converted in an intensity particle size distribution with ZetaSizer Software 7.10 version, based on the Stokes-Einstein equation. The zeta potential was quantified by laser Doppler electrophoresis (LDE) using polymer composite suspension with a concentration ranging between 0.1 and 0.001 gL^{-1}. The zeta potentials were automatically calculated from the electrophoretic mobility using the Smoluchowski's approximation. For each sample, the statistical average and standard deviation of data were calculated from 8 independent measurements each with 20 runs.

The polymer composite samples were homogenized with a bath sonicator for 40 min to allow a good dispersion without damaging the polymer materials. A tip ultrasound probe (Branson Model 250) delivering pulses of 20.000 kHz at 35% of its nominal power (350 W) was subsequently applied. The duration of each pulse was 5 and 10 minutes. Each pulse lasts 0.1s and is followed by a rest time of 0.1 s.

Acid-base properties determination by titration experiments.

Samples with a concentration of 1 gL^{-1} of MPLH, MP, Lig-H were studied with potentiometric evaluation by using a pH meter (Schott instruments, model Handylab pH 11) using different solutions; acid solutions of 0.1 M and 0.5 M HCl and on the other hand, two basic solutions of 0.1 M and 2 M NaOH. The pH meter

was calibrated with buffer solutions of pH 4, 7 and 10. The potentiometric curves were obtained by measuring the change in pH after each addition of base and acid solution, respectively; the additions were made slowly with continuous stirring.

RESULTS AND DISCUSSION

For the sake of comprehensiveness, in the first part of the results and discussion section, we show a complete study of the preparation conditions of the novel nanoparticles along with their physical and chemical characterization in both solid-state and in aqueous suspension. In the second part of this section the electrochemical analysis of the nanoparticle composite materials showing the highest dispersion in water is presented.

Figure 1 shows the TEM images of the polymer composites studied. The polymer materials are a series of composites containing either two or three macromolecules. These materials largely comprise individual particles exhibiting spherical morphology with sizes ranging between 200 nm for polymers made of methyl-cellulose and polypyrrole (MP, Figure 1A) to 20 nm in diameter for those materials containing methylcellulose, polypyrrole and highly sulfonated lignin biopolymer (MPLH, Figure 1B). The latter composites have a distinctive hierarchical structure with individual polymer nanoparticles assembled in strands or chains such as *necklace beads* (Figures 1B.1 and 1B.2). Interestingly, when lignin was present, the size of each polymer nanoparticle comprising the strands was one order of magnitude smaller than in MP materials containing two components. The presence of cellulose appears to be essential in both the genesis of each nanoparticle and their assembling along the polymer strand. Cellulose might be acting as a substrate during the initial growth of the conjugated polymer, thereby favouring the incorporation of pyrrole and their subsequent polymerization into the nanoparticle network [17]. The cellulose was probably also a binding agent favoring the connectivity of each nanoparticle along the chains. In addition, cellulose seems to have an impact on the particle aggregation; the absence of cellulose seems to provoke the loss of sphericity of

the nanoparticles as it was observed for those samples made of polypyrrole and highly sulphonated Lignin (PLH, Figure 1C).

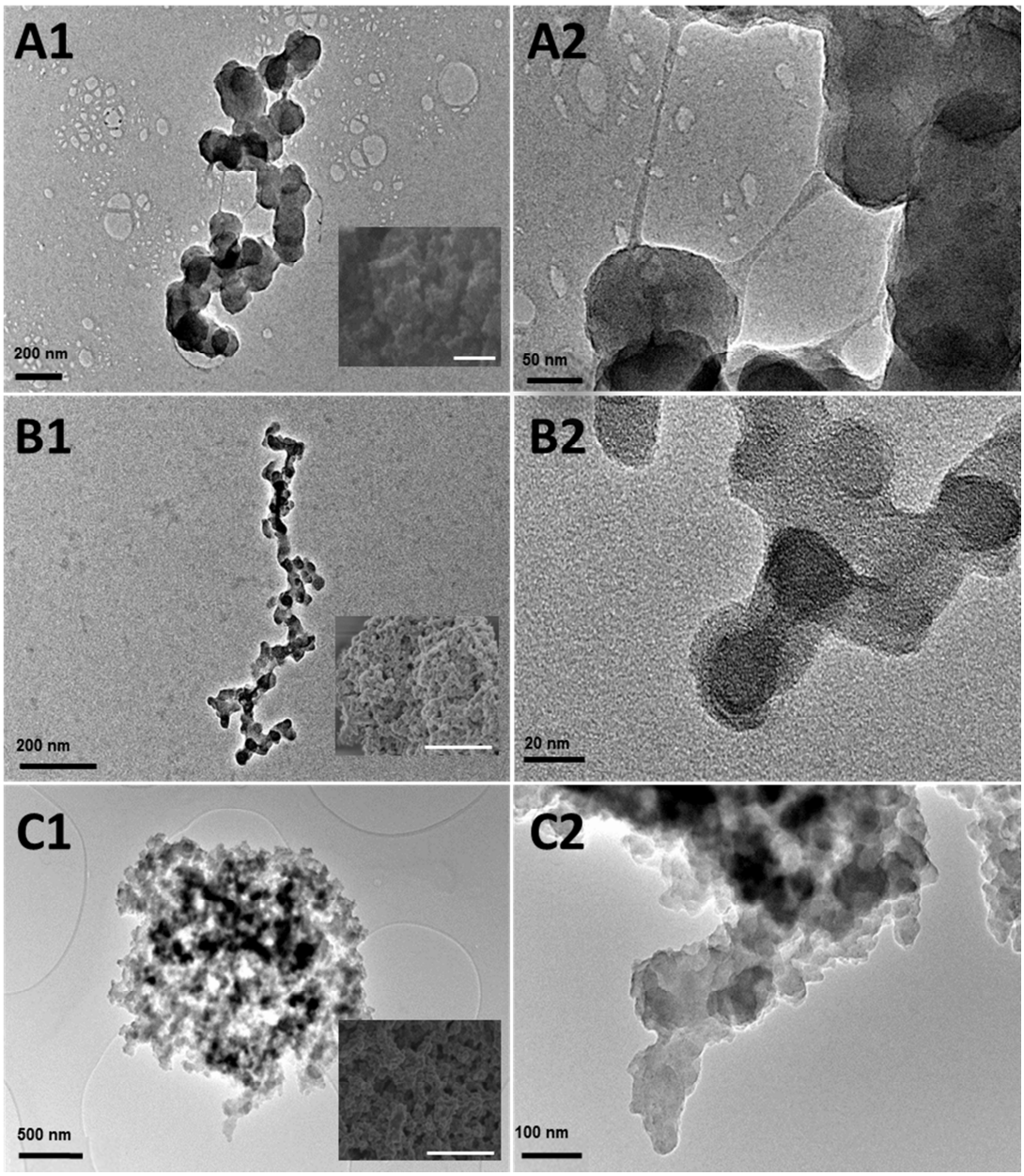

Figure 1. Transmission electron microscopy images of the different particulate polymer composite materials: MP **A),** MPLH **B)** and PLH **C)**. A2, B2, and C2 refer to the zoomed area´s from A1, B1 and C1 respectively Inset: Corresponding SEM images to each of materials. The scale bar on the SEM insets is 5 μm for A.1 and 1 μm for both B1 and C1.

We found that the PPy content, inferred from elemental analysis of nitrogen, is directly related to the amount of sulfur from the sulphonic groups in the lignin biopolymer as shown in Figure 2A. The estimated amount of PPy within the MPLX series shown the tendency: MPLH (19.8 wt. %) > MPLM (11.1 wt. %) >

MPLL (5.8 wt. %). From this trend, we deduced that the interactions between the positive charges in the five-member ring of the pyrrole monomer and the negative charges from the sulphonic anions anchored in the lignin chains might govern a highly efficient assembly between the two networks during polymerization. Besides, it has been reported that sulfonate moieties solubilizes organic substances in aqueous solutions, which might also enable the incorporation of the PPy polymer in the composite [18]. Regarding the role of cellulose in the chemical composition of the polymer, MPLH composite show higher nitrogen content than in PLH (16.9 wt. % PPy) where cellulose was absent.

The content of redox-active quinone was estimated by electrochemical analysis of thin-film polymer composite electrodes. Because MPLH and PLH composite materials show the highest amount of PPy in their composition they were chosen as the most suitable candidates for further investigations. Figure 2B shows the voltammetric response for an MPLH sample with current values normalized to scan rate (more details in Figure S1). We assign the peak at 0.55 V vs Ag/AgCl to the lignin biopolymer as the potential agrees well with previously reported formal potentials of lignin. The capacitive response in the region -0.2 and +0.3 V vs Ag/AgCl is ascribed to doping of the PPy component of the composite. As typical for PPy electrochemistry there is a doping on-set around -0.4 V vs Ag/AgCl [19]. The dependence of both, oxidation and reduction absolute peaks current with scan rate for MPLH and PLH electrodes are displayed in the inset plot in Figure 2B and Figure S2, respectively. The corresponding slopes are between 0.7 and 0.8. Similar dependence on both oxidation and reduction peaks and slope values were found for the PLH sample (Figure S2 and Table S4). The integration of the lignin peak, after subtraction of a linear base-line, indicates a lower capacity for PLH than for the MPLH electrode (Table S5). For MPLH a quinone capacity of 1.6210^{-5} C corresponding to $1.68\ 10^{-10}$ mol charges was evidenced. This value is higher compared to the corresponding quinone capacity in PLH which was evaluated to $5.33\ 10^{-6}$ C corresponding to $5.52\ 10^{-11}$ mol charges per 2.5 µL suspension used in the preparation of the thin-film electrodes. The remaining charge was assigned to PPy and was evaluated to 350

C g^{-1} in PHL, a value more than twice the value found for the highly-water dispersible MPLH composite material (157 C g^{-1}).

In order to reveal the spatial distribution of each macromolecule in the composite material, we performed energy-dispersive X-ray spectroscopy (XEDS) of nitrogen, sulfur and carbon elements while operating in ADF-STEM mode in the transmission electron microscope. Figure 2C shows a homogeneous distribution of the three components along with the nanoparticles that form the chain confirming that the three macromolecules networks were homogeneously interpenetrated in MLPH composite. Analysis of the distribution of sulfur and nitrogen in the PLH composite also confirmed the homogeneous distribution of polypyrrole and lignin in the nanoparticles of the chains as it is shown in Figure S3. We have also evidenced by UV-vis spectroscopy (Figure S4) a redshift in the absorption band corresponding to the π-π* transition from 280 nm to 286 nm in lignin biopolymer and in MPLH, respectively. This fact confirms the enhancement of π-π interactions between lignin chains in the composite as a result of the close chemical and electronic coupling at the nanoscale among the different constituents of the metal-free polymer system [20].

The development of low-cost multifunctional electrode materials will require precise control of their textural properties to facilitate specific molecular interactions of the particle surface and chemical species such as water, carbon dioxide, oxygen, hydrogen or electrolyte ions. Figure 2D shows a comparison between the gas adsorption isotherms for a series of polymer composites. The isotherms clearly show the impact of the polymer composition on the gas up-take capacity of the composite material and, as expected, a trend is observed regarding the volume of the adsorbed gas, the pore size and the surface area (Table S6). For example, the hybridization of the methylcellulose with the conjugated polymer increases the pore size from 0.69 nm to 0.77 nm. The presence of sulphonic groups in the lignin biopolymer has a strong impact on the gas adsorption and textural properties of the MPLX composites series observing a gradual drop on the surface area as the content increase. Moreover, there was a clear relation between the sulphonic content and the final morphology of the

composites as it is shown in Figure S5, in comparison with the PPy and MP materials.

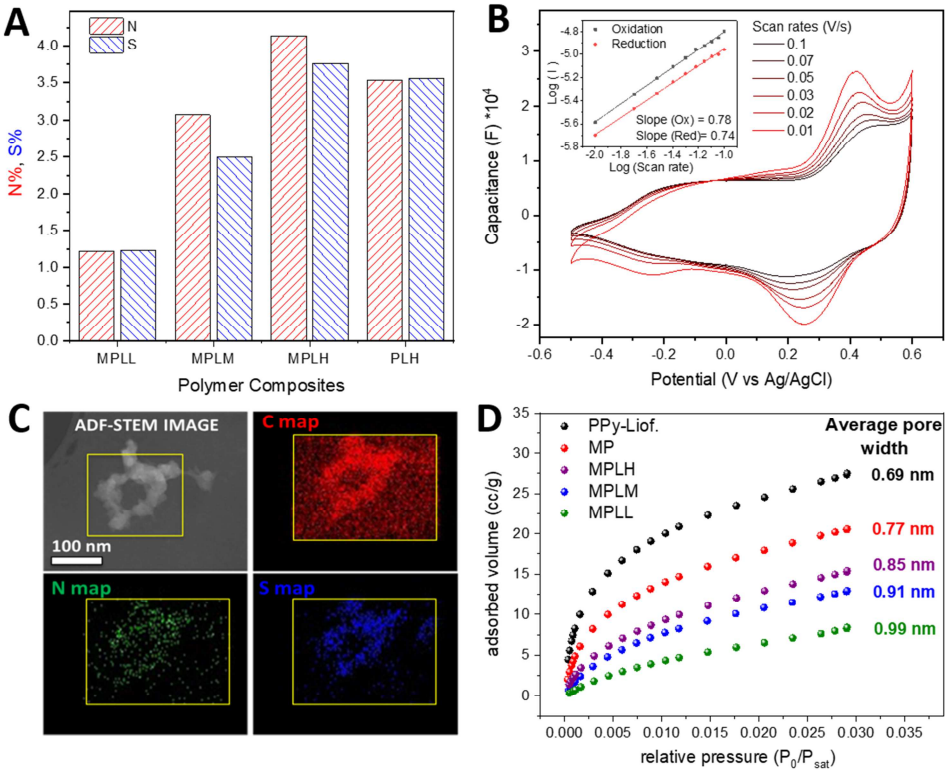

Figure 2. Nitrogen and sulfur content determined by elemental analysis **A)**. Cyclic voltammetry of a thin-layer of MPLH electrode showing the current normalized at different scan rates **B)**. Inset: log (Absolute peak currents) as a function of log (scan rate) of oxidation (black curve) and reduction (red curve) process of MPLH. MPLH layers were then characterized electrochemically in 1 M $NaCl_{aq}$ buffered with 10 mM Na_2HPO_4 and 10 mM H_3BO_3 to pH 4.3 and purged with N_2 for 20 min**.** ADF-STEM image of MPLH and XEDS maps showing the chemical distribution of the different elements (C-red, N-green, S-blue) within the structure of the MPLH nanohybrid **C)**. CO_2 gas adsorption isotherms for the polymer material systems studied in this work **D)**.

After the initial characterizations of the different materials MPLH and PLH were chosen as the optimal candidates for the target application. Figure 3 shows the impact of the chemical composition of the polymer materials on the particle size distribution, the acid-base properties, and the zeta potential values. Figures 3A and 3B show the particle size distribution corresponding to MPLH and PLH composites, respectively, determined by dynamic light scattering (DLS). As can be seen, the aggregate size distributions of each polymer composite show similar average values (~ 500 nm) in water after sonication for 15 minutes. The MPLH

composite shows improved long-term stability in water compared to the PLH sample that precipitated after a few minutes, corroborating the strong influence of the cellulose polymer in the stability of the composite suspensions. In addition, the polymer composites enclosing lignin with medium and low content of sulphonic groups exhibited larger aggregate sizes than those composites containing highly sulfonated lignin (Figure S6).

Figure S7 shows the zeta potential for the series of polymeric samples at different concentrations in water. The PPy and MP suspensions exhibited positive zeta potentials, while samples containing lignin showed negative zeta potentials. We attribute this effect to a higher impact of the negative charges of the sulfonic groups than the positive charges from polypyrrole on the surface. In fact, as the PPy-content increases, the zeta potential value also increases towards more positive values balancing the total charge.

Figure 3C shows the correlation between the ionization constant (pK) and the zeta potential values at different pH for an MPLH polymer suspension. We found a pH region with two pK constants (pK ≈ 1.5 and 9) in agreement with the change of zeta potential observed at acidic and basic pH. A 1 g l^{-1} suspension of MPLH particles dispersed in deionized water is negatively charged, with a zeta potential value close to -30 mV and a pH value of approximately 4. In the pH range comprising the two ionization constants, this suspension preserves its stability even though a tiny amount of acid/base can easily change its pH. So, there was not a correlation between the acid-base properties, the zeta potential values and the permanence in the suspension of the MPLH composite particles. Out of this range ($1.5 \leq pH \geq 9$), the polymer particles progressively lose their stability and do not remain in suspension. Therefore, the precipitation of the polymer composite particles in aqueous media might be due to the hydrolysis of the methylcellulose polymer at low and high pH values, respectively. In addition, pH variations show negligible effects on cellulose with constant zeta potential values and no indications of titrations (Figure S7 and S8). So, the acid-base character and the charge surface values of the particles must be mainly governed by the synergistic combination of the physical and chemical properties at the nanoscale of the PPy and lignin macromolecules, being this interaction also

mediated by the presence of the cellulose. Intriguingly, the presence of cellulose did not affect negatively the electrochemical properties of the redox moieties present in the lignin biopolymer as it is shown in Figure 4.

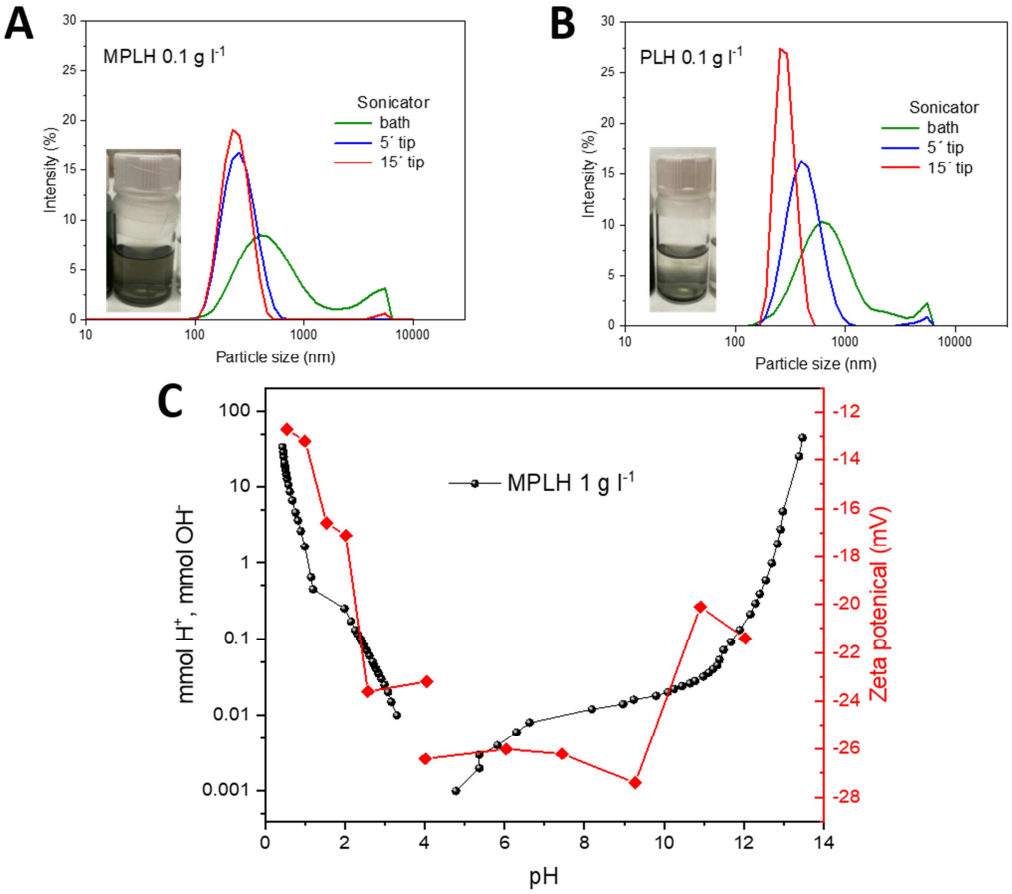

Figure 3. Characterization by dynamic light scattering (DLS) of the polymer composite suspensions containing MPLH **A)** and PLH **B)**. Correlation between the acid-base properties measured by titration and the zeta potential values for MPLH material **C)**.

Figure 4A shows the cyclic voltammograms (CVs) for a suspension of the MPLH composite particles in an aqueous solution at different pH values. The voltammograms exhibit one principal redox peak over the pH range 0.8-3.7 corresponding to the reversible redox reaction of the catechol moieties in the lignin biopolymer as it is shown in Scheme 2. Figure 4B shows the cyclic voltammetry for the MPLH nanoparticles suspended in an aqueous acidic media saturated with CO_2 gas. Interestingly, two electrochemical processes are displayed, both occurring at positive potential. The redox process at higher potential, *Process I,* corresponds to the above-mentioned redox reaction of the

catechol units in lignin; the other reaction occurring at a lower potential, *Process II*, could be attributable to catechol units with substituents containing more oxygen groups such as methoxy groups or neighboring C_9-O- groups directly connected to the phenyl ring [21]. Because of the strong electron-donating effect of the oxygen atoms bonded to the aromatic ring, a significantly lower redox potential than for *Process I* was observed. Several causes for this unusual electrochemical behavior were considered such as the hydrogen gas generation by the reduction of protons to molecular hydrogen and also the electroreduction of CO_2. However both possibilities were discarded due to the following described results: (i) In order to investigate the participation of hydrogen, a galvanostatic reduction of an aqueous suspension (pH ~ 1) of MPLH material ($1gL^{-1}$) was carried out in an electrolyzer cell comprising three compartments separated each of them by a Nafion® 117 membranes (Figure S9). The use of this experimental setup prevented dissolution, migration, and deposition of Pt nanoparticles from the counter electrode to the surface of the working electrode as well as the interference of H_2 gas, produced also by the catalytic activity of Pt. After cycling during more than 7 hours at 0.25 mA, the solid polymer nanoparticles were decanted and the liquid supernatant phase analyzed by liquid proton NMR in an air-free tube [22]. The absence in the spectra of the resonance corresponding to molecular hydrogen confirmed that *Process II* is not due to a reversible hydrogen reaction formation (Figure S10). This result was expected, as the thermodynamic potential for hydrogen evolution is much lower than the experimental one observed here under similar acidic conditions [23]. Moreover, we have also shown, by cyclic voltammetry, that the potential where H_2-formation occurs does not correspond to the potential for *Process II.* (Figure S11). (ii) We have also discarded the possibility of CO_2 reduction at the potential window applied in the present study, because in general the redox potential at which the CO_2 reduction takes place in aqueous systems has been determined close to -0.48V vs. Ag/AgCl [24]. Furthermore, as it is shown in Figure S11 only below 0 V vs. Ag/AgCl (aprox. -0.4V vs. AgCl) an irreversible process that might be due to CO_2 reduction was observed. Therefore, the reorganization of the interpenetrated polymer network in the presence of CO_2 is considered as the most plausible reason to explain the amplification of *Process II*.

Regarding the participation of CO_2, we observed that the presence of CO_2 lead to an enhancement of the absolute magnitude of the anodic and cathodic peak-heights of *Process I* in the MPLH composite (Figure S12). Moreover, when lignin is *nanoconfined* into the MPLH-particle an anomalous pH-dependence of the equilibrium potential for the *Process I* was found, as shown in Figure 4C. Two well-defined regions exhibiting two different slopes were evidenced independently in the presence of CO_2. The slope of the equilibrium potential as function of pH was -4 mV pH^{-1} in the pH range between 1.2 and 3.5 in the presence of CO_2. This value, closer to zero, might indicate that both the oxidized and reduced forms in lignin are fully deprotonated or that the local pH at the surface of the polymer composite might be buffered due to the presence of dissolved CO_2. For *Process II* occurring in the MPLH particles, the formal potential in the presence of CO_2 shows a linear pH dependence. For the *non-confined* lignin biopolymer the equilibrium potential of the *Process I* is pH-dependent in the presence of CO_2 in the whole pH-range (Figure S13). In fact, the average slope of the equilibrium redox potential versus pH over the pH range 0.5–4.6is −49 mV pH^{-1} unit, which is close to the value of −59 mV pH^{-1} expected from a two-electron, two-proton process. The linear fit to the data between pH 0.9-3.5 for the *Process II* revealed a slope value of -98 mV pH^{-1}. Moreover, the intensity of the anodic and cathodic peaks corresponding to the reorganized lignin moieties follows a linear dependence with pH as shown in Figure 4D. Remarkably, the presence of carbon dioxide boosted the second process reaction by 500 % at a pH value of 0.8.

We performed the same electrochemical experiment for a solid electrode of MPLH composite material with and without CO_2. In that case, there was no evidence of second redox process (Figure S13). The occurrence of three redox stages corresponding to the presence of two redox processes was only observed when the polymer nanoparticles were in suspension. The main reason behind this behavior might be the relatively large sample volume of the particles in suspension compared to the situation in the solid electrode set-up. Effectively this means that electrochemical conversion might be only related to a thin layer close to the polymer surface, which is in good agreement with the above

mentioned result. In suspension, nanoparticles that are in contact with the surface of the electrode are being constantly replaced by fresh material that was converted during cycling.

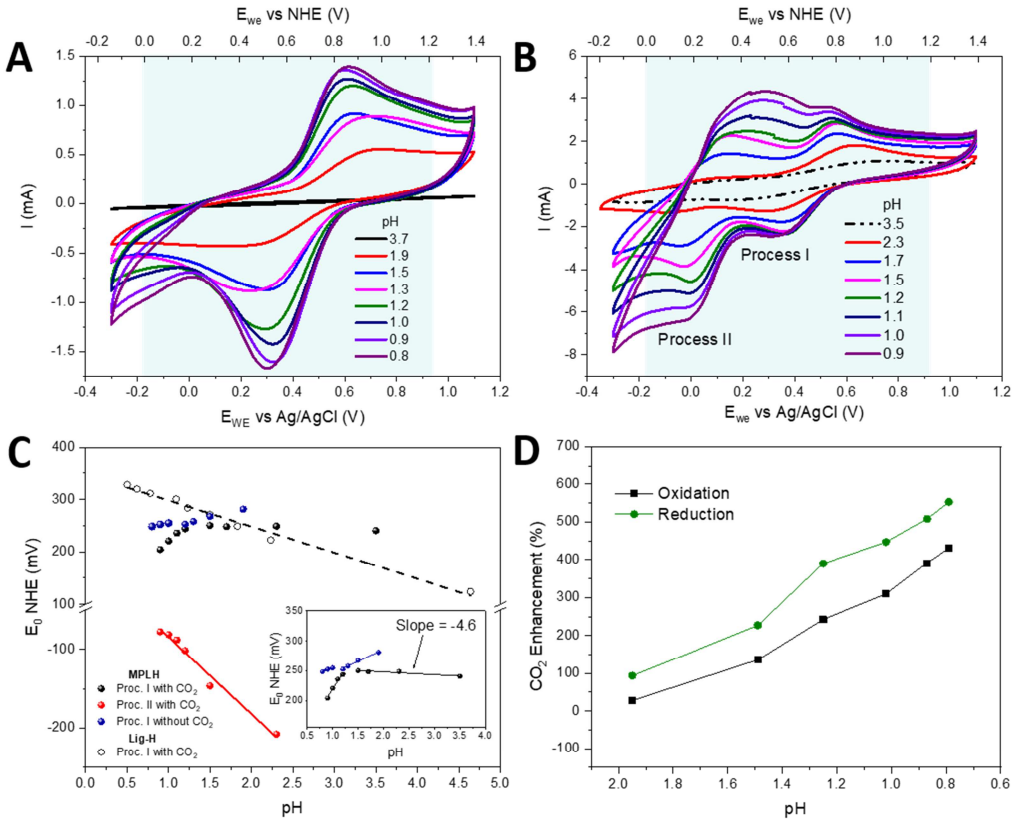

Figure 4. Electrochemical characterization of the polymer composites suspensions by using a three-electrode cell configuration. Cyclic voltammograms in an aqueous acidic media without **(A)** and with CO_2 **(B)** of the MPLH polymer composite suspensions. The Purbaix diagram of MPLH water-based suspensions with and without CO_2 **(C)**. Anodic and cathodic currents for the reversible transformation of *Process II* in the presence of CO_2 **(D)**. (Pt wire was used as a counter electrode and Ag/AgCl as a reference electrode; Scan rate = 10 mV s^{-1}).

Figure 5 shows the proposed mechanism to explain the electrochemical behavior observed in the polymer composite nanoparticles with and without the presence of CO_2 gas at different pH values. As stated above, the electrochemical processes most probably occur at the surface. Then, when the MPLH nanoparticles are placed in deionized water, the pH value is close to 4 and the surface charge value is -30mV. These values are mainly produced by the presence of hydrated sulfonic groups on the surface of the particle. At this point, it hardly observes any redox process due to the slow kinetics of the reaction provoked by the deficiency of

protons (Figure 5A). If the suspension is acidified, *Process I* emerges. Also, the zeta potential increases and becoming more positive. This change in the average value of the surface-charge suggests that part of the sulphonic groups initially doping the polypyrrole now tends to face the nanoparticle´s surface, interacting electrostatically with the protons and water molecules from the solution. Under these conditions a spatial alteration of the interpenetrated polymer network at the surface of the nanoparticles might occur (Figure 5B). When CO_2 is added, noticeable changes are reflected in the CV such as the appearance of the *Process II* coexisting with the *Process I*. Besides, the electrochemical reduction of the quinone to hydroquinone in *Process I* will favor an increase of the pH value near the surface due to proton consumption [25]. This situation will most probably favor the formation and stabilization of the HCO_3^- anion at the liquid/solid interphase. This situation might also be favoring structural rearrangement of the interacting macromolecules along the interpenetrated network [26]. Then, the polypyrrole may act as an electrophile interacting with the bicarbonate anion forming a stable adduct, then changing their physical and chemical interrelation with the biopolymers (Figure 5C) [27]. The possible formation of a carbonate between the CO_2 molecule and the semiquinone which can then be protonated at low pH in an aqueous media [28] and appear o consume protons promoting also the rearrangement of the interpenetrated polymer network can not be discarded. Therefore, here CO_2 is not electroreduced and is simply acting as a precursor of the species formed after hydration [24].

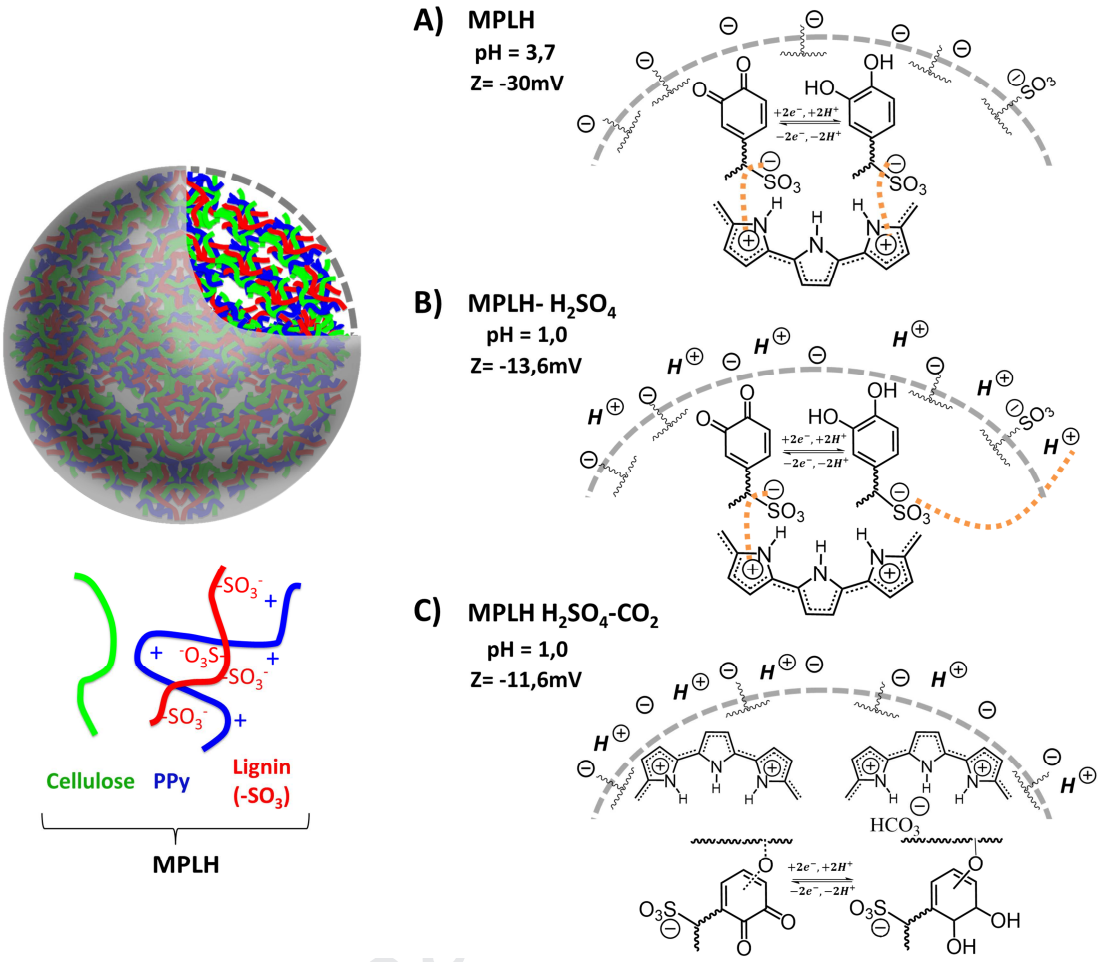

Figure 5. The proposed mechanism to explain the presence of three redox stages in the polymer composite nanomaterial in the presence of CO_2.

CONCLUSION

We have devised a new sustainable multifunctional nanomaterial that utilizes CO_2 as a useful resource to reversibly store charge. The novel material is a hierarchically-structured polymer composite that is made of inexpensive and environmentally friendly macromolecules such as methylcellulose, which assisted the creation of the nanoparticles during the colloidal polymerization and also endorsed long-time stability to the polymer active suspensions in water. From cyclic voltammetry measurements, two main reversible processes were observed corresponding to the redox reaction of the lignin biopolymer. The process at the lower potential is enhanced by up to 500 % by the presence of carbon dioxide. The novel properties might be originated from an intimate chemical and electronic connection at the nanoscale among the different

components of the polymer composite and the structural rearrangement of the lignin biopolymer by the incorporation of CO_2. This creative strategy envies multiple advantages such as the utilization of low-cost raw materials and sustainable pathways for designing advanced functional nanomaterials; the application of greenhouse gases such as CO_2 to promote bifunctionality by the same active nanostructured material dispersed in water making cost-effective storage system. The proposed metal-free polymer composite–CO_2 system could potentially serve as a new CO_2 utilization technology in the time of pursuing sustainable and environmentally friendly energy storage systems for the future.

ASSOCIATED CONTENT

Supporting Information

The Supporting Information (experimental details, supporting tables and figures) is available on the Elsevier website.

AUTHOR INFORMATION

Corresponding Author

*E-mail: jcarretero@ictp.csic.es

ORCID

Daniel Arenas-Esteban: 0000-0002-5626-9848
David Ávila-Brande: 0000-0003-0452-2482
Miguel A. López-Manchado: 0000-0002-2425-4000
Javier Carretero-González: 0000-0002-8008-5715

ACKNOWLEDGMENT

J.C.G. acknowledges support from the Spanish Ministry of Economy, Industry, and Competitiveness (MINECO) through a Ramon y Cajal Fellowship (RYC-2015-17722) and the Retos Project (MAT2017-86796-R, AEI/FEDER/UE). D.A.E. and D.A.B acknowledge the Retos Project (MAT2017-84385-R, AEI/FEDER/UE). P.N. acknowledges the postdoctoral contract from the Government of the Comunidad de Madrid (CAM, PEJD-2018-POST/AMB-9248). M.L.M. and J.C.G. acknowledge

the PTI-FLOWBAT project (Ref. Nº: 201980E101) from the Spanish Research Council (CSIC).

Notes

An European patent application (EP19382731) has been filed by Consejo Superior de Investigaciones Científicas naming A.F.B., G.R, D.R.C., M.L.M and J.C.G. as inventors.

Graphical Abstract

A wooden rechargeable electrolyte nanomaterial

A new sustainable multifunctional nanomaterial exhibits well-controlled three redox stages in the same component unit when electrochemically cycled in saturated CO_2 aqueous conditions. The low-cost advanced nanomaterial offers the opportunity to address two main energy and environmental challenges: global warming and polluting atmosphere from greenhouse gas emissions and the generation of electricity along with energy storage from renewable sources.

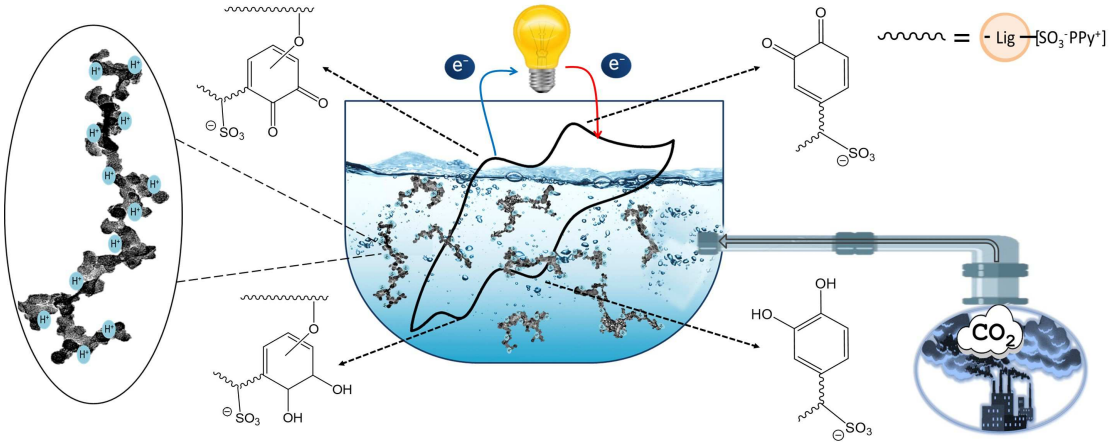

REFERENCES

[1] EUROPEAN COMMISSION Climate Action. Annual Conference of Parties (COP) at COP21 at Stade de France (Gate E) in Paris (7–8 December (2015). http://ec.europa.eu/clima/policies/international/negotiations/paris/index_en.htm.

[2] S. Chu, Y. Cui and N. Liu, The path towards sustainable energy, *Nature Materials*, 16 (2017) 16–22. https://doi.org/10.1038/nmat4834

[3] D. Larcher and J-M. Tarascon, Towards Greener and More Sustainable Batteries for Electrical Energy Storage, *Nature Chemistry*, 7 (2015) 19–29. https://doi.org/10.1038/nchem.2085

[4] A. S. Aricó, P. Bruce, B. Scrosati, J-M Tarascon and W. van Schlkwijk, Nanostructured materials for advanced energy conversion and storage devices, *Nature Materials*, 4 (2005) 366–377. https://doi.org/10.1142/9789814317665_0022
[5] B. Kang and G. Ceder, Battery materials for ultrafast charging and discharging, *Nature*, 458 (2009) 190–193. https://doi.org/10.1038/nature07853
[6] G. Milczarek and O. Inganäs, Renewable cathode materials from biopolymer/conjugated polymer interpenetrating networks, *Science,* 335 (2012) 1468-1471. http://doi.org/10.1126/science.1215159
[7] C. K. Chan, H. Peng, G. Liu, K. McIlwrath, X. F. Zhang, R. A. Huggins and Y. Cui High-performance lithium battery anodes using silicon nanowires, *Nature Nanotechnology*, 3 (2008) 31–35. https://doi.org/10.1038/nnano.2007.411
[8] K. B. Hatzell, M. Boota and Y. Gogotsi, Materials for suspension (semi-solid) electrodes for energy and water technologies, *Chem. Soc. Rev.*, 44 (2015**)** 8664. https://doi.org/10.1039/C5CS00279F
[9] M. Duduta, B. Ho, V. C. Wood, P. Limthongkul, V. E. Brunini, W. C. Carter, and Y-M. Chiang, Semi-solid lithium rechargeable flow battery, *Adv. Energy Mater.*, 1 (2011) 511–516. https://doi.org/10.1002/aenm.201100152
[10] P. Leung, A. A. Shah, L. Sanz, C. Flox, J. R. Morante, Q. Xu, M. R. Mohamed, C. Ponce de León, F. C. Walsh, Recent developments in organic redox flow batteries: A critical review, J*. Power Sources*, 360 (2017) 243–283. https://doi.org/10.1016/j.jpowsour.2017.05.057
[11] W. Yan, C. Wang, J. Tian, G. Zhu, L. Ma, Y. Wang, R. Chen, Y. Hu, L. Wang, T. Chen, J. Ma and Z. Jin, All-polymer particulate slurry battery, *Nature Communications,* 10 (2019) 2513.
https://doi.org/10.1038/s41467-019-10607-0
[12] T. Janoschka, N. Martin, U. Martin, C. Friebe, S. Morgenstern, H. Hiller, M. D. Hager and U. S. Schubert, An aqueous, polymer-based redox-flow battery using non-corrosive, safe, and low-cost materials, *Nature*, 527 (2015) 78–81. https://doi.org/10.1038/nature15746
[13] E. C. Montoo, G. Nagarjuna, J. Hui, M. Burgess, N. M. Sekerak, K. Hernández-Burgos, T.-S. Wei, M. Kneer, J. Grolman, K. J. Cheng, J. A. Lewis, J. S. Moore, and J. Rodríguez-López, Redox Active Colloids as Discrete Energy Storage Carriers, *J. Am. Chem. Soc.*, 138 (2016) 13230–13237. https://doi.org/10.1021/jacs.6b06365
[14] G. Milczarek, Preparation and characterization of a lignin modified electrode *Electroanalysis*, 19 (2007) 1411-1414. https://doi.org/10.1002/elan.200703870
[15] G. Nyström, A. Razaq, M. Strømme, L. Nyholm and A. Mihranyan, Ultrafast all-polymer paper-based batteries, *Nanoletters*, 9 (2009) 3635-3639. https://doi.org/10.1021/nl901852h
[16] F. Stoeckli, E. Daguerre, A. Guillot, The development of micropore volumes and widths during physical activation of various precursors, *Carbon,* 37 (1999)2075–2077. http://dx.doi.org/10.1016%2FS0008-6223(99)00220-1
[17] A. Razaq, A. Mihranyan, K. Welch, L. Nyholm and M. Stromme, Influence of the Type of Oxidant on Anion Exchange Properties of Fibrous *Cladophora* Cellulose/Polypyrrole Composites, *J. Phys. Chem. B*, 113 (2009) 426-433. https://doi.org/10.1021/jp806517h

[18] B. Zinger, Electrochemistry of quinoid dopants in conducting polymers, *Synthetic Metals*, 30 (1989) 209-225. https://doi.org/10.1016/0379-6779(89)90791-1
[19] H. Olsson, D. O. Carlsson, G. Nyström, M. Sjödin, L. Nyholm and M. Stromme, Influence of the cellulose substrate on the electrochemical properties of paper-based polypyrrole electrode materials, *J Mater Sci*, 47 (2012) 5317–5325. https://doi.org/10.1007/s10853-012-6418-y
[20] F. Xiong, Y. Han, S. Wang, G. Li, T. Qin, Y. Chen, F. Chu, Preparation and Formation Mechanism of Renewable Lignin Hollow Nanospheres with a Single Hole by Self-Assembly, *ACS Sustainable Chem. Eng.*, 53 (2017) 2273-2281. https://doi.org/10.1021/acssuschemeng.6b02585
[21] G. Milczarek, Lignosulfonate-Modified Electrodes: Electrochemical Properties and Electrocatalysis of NADH Oxidation, *Langmuir* 25 (2009) nº 17, 10345-10353. https://doi.org/10.1021/la9008575
[22] J. Y.-C. Chen, A. A. Martí, N. J. Turro, K. Komatsu, Y. Murata and R. G. Lawler, Comparative NMR Properties of H2 and HD in Toluene-d8 and in H_2/HD@C60, *J. Phys. Chem. B*, 114 (2010)14689-14695. https://doi.org/10.1021/jp102860m
[23] H. Ooka, M. C. Figueiredo and M. T. M. Koper, Competition between Hydrogen Evolution and Carbon Dioxide Reduction on Copper Electrodes in Mildly Acidic Media Langmuir, 33 (2017) 9307-9313. https://doi.org/10.1021/acs.langmuir.7b00696.
[24] C. Costentin, J. M. Sáveant and C. Tard, Catalysis of CO_2 Electrochemical Reduction by Protonated Pyridine and Similar Molecules. Useful Lessons from a Methodological Misadventure, *ACS Energy Lett.* 3 (2018) 695-703. https://doi.org/10.1021/acsenergylett.8b00008.
[25] M. J. Aziz and D. G. Kwabi, pH swing cycle for CO_2 capture electrochemically driven through proton-coupled electron transfer. Preprint at https://chemrxiv.org/articles/pH_Swing_Cycle_for_CO2_Capture_Electrochemically_Driven_through_Proton-Coupled_Electron_Transfer/7853414 (2019).
[26] G. Milczarek, Lignosulfonate‐Modified Electrode for Electrocatalytic Reduction of Acidic Nitrite, *Electroanalysis* 20, (2008) nº 2, 211-214. https://doi.org/10.1002/elan.200704071.
[27] M. F. Cunningham and P. G. Jessop, Carbon Dioxide-Switchable Polymers: Where Are the Future Opportunities?, *Macromolecules*, 52 (2019) 6801-6816. https://doi.org/10.1021/acs.macromol.9b00914
[28] Y. Liu, H. Ye, K. M. Diederichsen, T. V. Voorhis and T. A. Hatton, Electrochemically mediated carbon dioxide separation with quinone chemistry in salt-concentrated aqueous media. Nature Communications 11 (2020), Article Number: 2278. https://doi.org/10.1038/s41467-020-16150-7.

Declaration of interests

X The authors declare that they have no known competing financial interests or personal relationships that could have appeared to influence the work reported in this paper.

☐The authors declare the following financial interests/personal relationships which may be considered as potential competing interests: